Applied Surface Science 258 (2012) 2910–2913

Contents lists available at SciVerse ScienceDirect

Applied Surface Science

journal homepage: www.elsevier.com/locate/apsusc

Ion trajectories and shadow effects in mesh-assisted plasma immersion ion implantation of insulator

Yongxian Huang[a,*], Xiubo Tian[a], Shixiong Lv[a], Shiqin Yang[a], R.K.Y. Fu[b], Paul K. Chu[b], Jinsong Leng[c], Yao Li[c]

[a] State Key Laboratory of Advanced Welding and Joining Harbin Institute of Technology No. 92, West Da-Zhi Street, Harbin 150001, Heilongjiang, People's Republic of China
[b] Department of Physics and Materials Science, City University of Hong Kong, Tat Chee Avenue, Kowloon, Hong Kong
[c] Center for Composite Materials and Structures, Harbin Institute of Technology, Harbin 150001, People's Republic of China

ARTICLE INFO

Article history:
Received 13 October 2011
Received in revised form 30 October 2011
Accepted 1 November 2011
Available online 10 November 2011

Keywords:
Ion trajectory
Shadow effect
Mesh-assisted plasma immersion ion implantation
Insulator
Particle-in-cell

ABSTRACT

A two-dimensional particle-in-cell (PIC) model considering secondary electron emission (SEE) as a function of ion instantaneous incident energy is developed for describing ion trajectories and shadow effects in mesh-assisted plasma immersion ion implantation (PIII) of insulator. The simulation results indicate that mesh-assisted PIII can improve the equivalent surface potential, suppress the emission of secondary electrons and provide better implantation dynamics for ions implantation on insulator. On 5 mm thick polymer substrate, an aluminum plasma implanted coating is achieved with excellent adhesion strength by mesh-assisted PIII with 10 mm mesh height. Consistent results are obtained from experiments and numerical simulation disclosing that shallow effects can be eliminated, and ions incident energy is enhanced.

1. Introduction

Plasma immersion ion implantation (PIII) of dielectrics could become a true challenge with the growing use of silicon on insulator (SOI) substrate in integrated circuit fabrication, and the world-wide development of flat panel display technology [1,2]. In both cases, the doping of silicon must be performed on silica or glass substrates with thicknesses in the millimeter range. However, attempts to implant insulating/dielectric substrates using PIII have encountered intrinsic physical limitations, such as charging, arcing and the difficulty of controlling the surface potential of the target [3,4]. The common PIII approach is to place the dielectric samples on a conductive substrate holder which connects with high-voltage pulses [5]. However, the magnitude of the potential at the dielectric–plasma interface is reduced by a combination of dielectric capacitance and charge accumulation due to the introduction of positive ions and emission of secondary electrons (SE) [1,5,6]. If the pulse length is long enough and/or the plasma density high enough, the insulator will charge up to the floating potential [7]. Thus, the insulating substrate that is positioned on a conducting target holder cannot rise to the full (negative) pulse bias potential, consequently, the effective implant energy is consequentially reduced [4,8]. The surface charging, electrical arcing, plasma sheath distortion, capacitance effects are common challenges for PIII on an insulating/dielectric material [6,9,10].

The effective dielectric thickness of the substrate and applied pulse length and frequency that can be used in practice are limited. Severe potential is significantly reduced and instrumental arcing may become too difficult to overcome [4]. To minimize surface charging and improve the depth of treatment, a metal mesh can be placed several mm or cm around the insulator and pulse biased together with the target holder [7,9,11–13]. In this way, a cage-shaped target forms and the insulating object inside the cage floats electrically. Ions accelerated across the sheath toward the mesh pass through the holes and are implanted into the insulator surface. The results show that mesh-assisted PIII is an effective technique for thick, complex shapes or large insulating objects [11,14–16]. The metal mesh not only improves the implantation energy and incident dose but also minimizes surface charging to some extent [7,9]. On the other hand, even with the mesh, ions accelerated through the mesh holes are not implanted at full potential [11], and it may be due to factors, such as ion deceleration between the mesh and insulator surface. The optimized dimension scaling of a mesh is also critical because if they are too large, ions implanted through the center region of the holes will not have high impact energy [11]. Besides, the distance between the mesh and insulator surface

* Corresponding author. Tel.: +86 451 86413951; fax: +86 451 86416186.
E-mail address: yxhuang@hit.edu.cn (Y. Huang).

0169-4332/$ – see front matter © 2011 Elsevier B.V. All rights reserved.
doi:10.1016/j.apsusc.2011.11.006

may also result in inefficient shielding of the drop in potential and ions may become decelerated once they get past the mesh. Proper placement of the mesh with respect to the insulator surface as well as correct dimensions and shape of the mesh holes are crucial to the ion energy. Moreover, shadowing effects due to the mesh are quite apparent and can affect the ion dose uniformity [17]. Therefore, the optimization of dimension scaling and height of mesh, and study of implantation dynamics including the evolution of surface potential and ion trajectories are critical for mesh-assisted PIII of insulator for achieving optimum dose uniformity and implanted ion energy.

2. Particle-in-cell model for mesh-assisted PIII of insulator

A 2D particle-in-cell (PIC) model considering secondary electron emission (SEE) as a function of instantaneous ions incident energy is developed for describing mesh-assisted PIII of insulator. The PIC model solves the Newton and Poisson equations. Kinetic, non-local and non-equilibrium effects have been included. Implanting ions with high energy can eject secondary electrons. The emission coefficient γ of SE is not constant and increases with instantaneous implanting energy $E_{\text{implanting}}$. In the model, the variation of γ with ion energy for dielectric materials is expressed approximately by

$$\gamma = \gamma_0 \sqrt{\frac{E_{\text{implanting}}}{E_0}} \tag{1}$$

where γ_0 is the coefficient corresponding to the implanting energy E_0. Thus, the variation of ion current $I_i(t)$ can be given by

$$I_i(t) = \left(1 + \gamma_0 \sqrt{\frac{E_{\text{implanting}}}{E_0}}\right) e u_i(t)\, n_i(t) \tag{2}$$

where e is the electronic charge, $u_i(t)$ is the velocity of ion, and $n_i(t)$ is the ion density.

Furthermore, because the sheath voltage usually reaches several kV, the sheath width rapidly increases, resulting in large displacement current due to the sheath expansion. Thus, the target current is composed of three currents: incident ion current, emitted electron current and displacement current [18]. The displacement current due to changing sheath potential and changing sheath capacitance are included.

$$I_d(t) = C_s(t)\frac{dV_s(t)}{dt} + V_s(t)\frac{dC_s(t)}{dt} \tag{3}$$

where $C_s(t) = \varepsilon_0 A/d_s(t)$ is the temporal capacitance, ε_0 is the dielectric permittivity of free space.

The target is assumed to be a nonconductor so that, on the time scale of applied pulse, charge in the dielectric accumulates, and cannot dissipate. The charge, in turn, builds up an opposing electric field that decreases the surface potential of the dielectric. Considering the charging and capacitance effects, the instantaneous surface potential surface potential is related to the dielectric properties and thickness of the insulating materials such that per unit area as given by

$$V_S(t) = V_0(t) - \frac{E_S(t)d}{\varepsilon_r} - \frac{\sigma(t)}{C_0} \tag{4}$$

where ε_r is the relative permittivity, E_S is the electric field in the plasma at the surface of the insulator, d is the thickness of the insulator, C_0 is the capacitance of per unit area. The surface charge density $\sigma(t)$ depends on the number of ion and SEE per unit area from the beginning of the present pulse. Hence, $V_S(t)$ can become more positive due to the charge accumulation if the relative permittivity ε_r is smaller and the sample thickness d is thicker.

For mesh-assisted PIII, the capacitance C is considered as the parallel capacitance of the insulator capacitance C_1 and C_2 between the insulator surface and mesh. The parallel capacitance can be given by

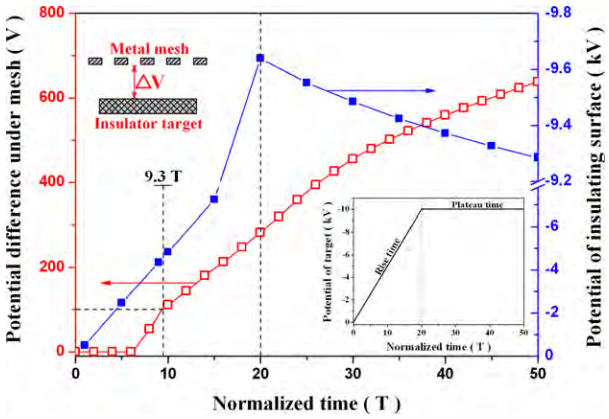

Fig. 1. Potential at the insulator–plasma interface and potential difference (ΔV) under the metal mesh as a function of time. The inset schematic diagram is the definition of ΔV, and the applied target potential is as shown in the lower-right inset.

$$C = C_1 + C_2 = \frac{\varepsilon_r \varepsilon_0 S_1}{d} + \frac{\varepsilon_0 S_2}{h} \tag{5}$$

where d is the thickness of the insulator, h is the mesh height above the insulator surface, S_1 and S_2 are the surface area of the insulator and mesh, respectively. Only the above surface of insulator and the nether surface of mesh are considered, so that $S_1 = S_2$. And then the capacitance of per unit area can be given by

$$C_0 = \frac{\varepsilon_r \varepsilon_0}{d_1} + \frac{\varepsilon_0}{h} \tag{6}$$

In the simulation, PIC simulation involves superparticles in a uniform grid of nodes, calculating the electrical fields at these nodes, and interpolating the forces on the particles. The movement of particles is described by Newton's laws [19]. We take Al^+ plasma and polymer insulator as an example in which all the base values of the input parameters, such as electron temperature $kT_e = 1$ eV, ion density $n_0 = 1 \times 10^{10}$ cm^{-3}, the relative permittivity of the insulator $\varepsilon_r = 3.4$, the thickness of the dielectric $d = 5$ mm, the amplitude of negative voltage pulse applied to the electrode $V_0 = -10$ kV, the rise time $t_R = 20\,\omega_{pi}^{-1}$ (where $\omega_{pi}^{-1} = (\varepsilon_0 m_i/n_0 q^2)^{1/2}$ is the inverse plasma ion frequency), and the emission coefficient of SE $\gamma_0 = 2$ corresponding to the ion incident energy $E_0 = 10$ keV.

3. Results and discussion

The temporal evolution of the surface potential of insulator and the potential difference ΔV (the ability of suppressing the emission of SE) under the mesh are calculated as shown in Fig. 1. Enshrouding the insulator substrate with a conducing mesh cage builds up an equipotential space between the mesh and insulator surface before implantation. The internal electric field under the mesh automatically builds up once plasma implantation starts. This field substantially suppresses the emission of SE from the insulator surface. At the time scale of 9.3 T ($T = (\varepsilon_0 m_i/n_0 q^2)^{1/2}$, the plasma ion period), the ΔV is 100 V, and the ability is enough to suppress SEE according to the lower energy of SE [20]. Ions implanted into the surface accumulate to produce a retarding electric field. The charge, in turn, builds up an opposing electric field which decreases the surface potential and enhances the ability of suppressing SEE for mesh-assisted PIII on insulator. Based on an overall consideration of the capability of the SE suppression and an increase of equivalent capacitance induced by the mesh,

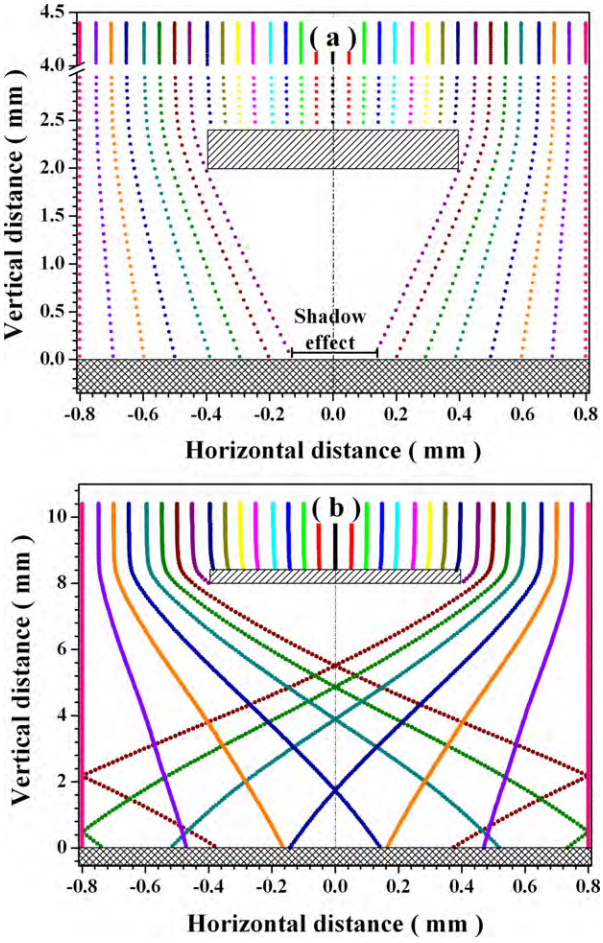

Fig. 2. Trajectories of ions on 2 mm plane above the mesh for different mesh height: (a) 2.0 mm and (b) 8.0 mm.

mesh-assisted PIII is to effectively accelerate the ions from the plasma and to retract SE thereby reducing surface charging.

For the first time, ions trajectories under the assisted mesh are specifically described as shown in Fig. 2. In order to disclose the dynamics of the implanted ions, seventeen ions with 0.05 mm distance at 2 mm plane above the mesh surface are real-time tracked. The marked ions move at the ion sound velocity before they encounter the plasma sheath. Fig. 1 depicts the complex ion trajectories for the mesh height $h = 2$ and 8 mm, respectively. The ions over the mesh bone are implanted into the mesh wall but not through the mesh into the insulator. When the height of mesh is too low, the divergence distance is small, and the shadow effect is quite apparent as shown in Fig. 2(a). With increasing the height of mesh, the divergence distance becomes larger, some ions run through different meshes space, and the shadow effect is weakened as shown in Fig. 2(b).

In order to disclose the shadow effect further, the marked ions, which locate as shown in the inset of Fig. 3, are tracked. In Fig. 3, the divergence of the marked ions is plotted as a function of the mesh height. When the mesh height is 8 mm, the divergence reaches more than one mesh unit length (1.6 mm) for the No. 1 ion. With the reducing of mesh height and the increasing of ions locating height, the divergence decreases as shown in Fig. 3. That is to say, the shadow effect is enhanced with the reducing of the mesh height, and more ions which are at higher location above the mesh will swell the shadow effect. Higher placement of the mesh with respect to the insulator surface is crucial to the ion dose uniformity. The

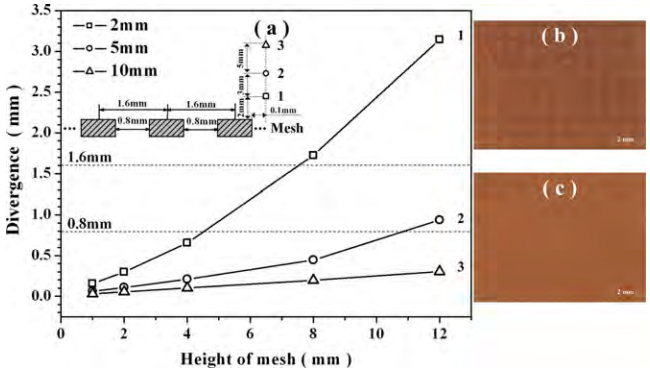

Fig. 3. Divergence of marked ions (Nos. 1–3) and shadow effects as a function of mesh height: (a) divergence of marked ions, (b) shadow effect with the mesh height 4 mm, and (c) shadow effect with the mesh height 10 mm.

influence law of shadow effect is proved by the mesh-assisted PIII of Al^+ plasma on polymer as shown in Fig. 3(b) and (c).

At the time scale of 100 T, the distribution of incident ions dose is shown in Fig. 4. The surface just under the mesh bone receives a lower ion dose due to the shadow effect of the mesh. This dose distribution remains the same trend for different mesh heights. However, with the increase of mesh height, more ions can round the mesh wall and implant into the insulator surface. The shadow effect is weakened with the increasing of the mesh height as shown in Fig. 4.

To corroborate the better implantation dynamics, a mesh-assisted aluminum PIII is performed on a polymer substrate with a thickness of 5 mm. Fig. 5 shows the typical fracture surface after scratching test using a diamond Rockwell head with 5 N loads. There are no large cracks and flaking morphology along the scratch track for mesh-assisted aluminum PIII. However, the distance of flaking expansion is more than 100 μm for the conversional aluminum PIII on the polymer. This means better adhesion between the implanted layer and polymer substrate due to the high energy ions implantation during mesh-assisted PIII. For the simulation data, as shown in Fig. 6, the percentage of high energy ($\geq$80% E_{max}) implanted ions is nearly equivalent to implantation of conductor, such as, at the timescale of 150 T, the percentages are 70.5% and 69.3% for conversional PIII on conductor and mesh-assisted PIII on insulator, respectively.

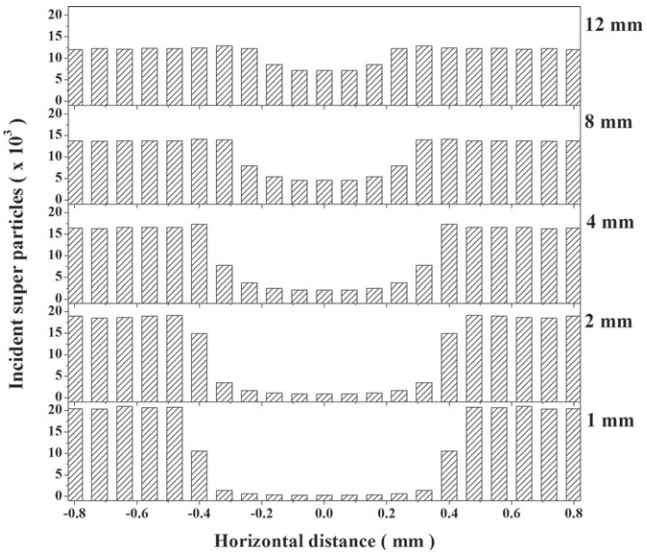

Fig. 4. Distribution of incident ions dose at the time scale of 100 T.

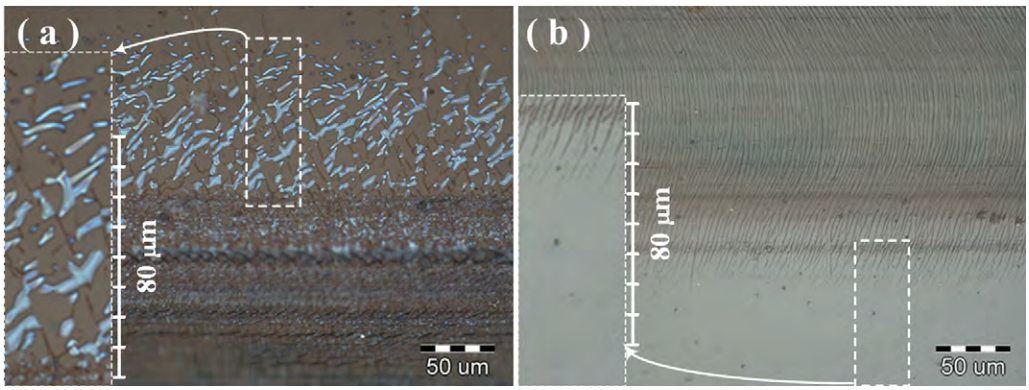

Fig. 5. Optical micrograph showing cracks of ions implanted layer on polymer after scratching test: (a) conversional aluminum PIII, and (b) mesh-assisted aluminum PIII with the mesh height 10 mm.

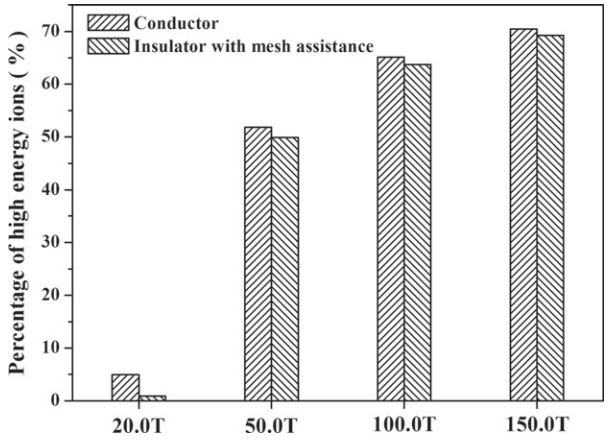

Fig. 6. Percentage of high energy ions at different time of one pulse.

The implantation dynamics has been studied by the 2D PIC model considering SEE as a function of ion instantaneous incident energy. For mesh-assisted PIII, the metal mesh has some positive effects on the plasma implantation dynamics. The equivalent capacitance is increased induced by the mesh compared to the insulator. The equivalent capacitance will retard the reduction of the surface potential assuming that the same charges are accumulated on the insulator. Consequently, the implantation efficacy can be improved [9]. Synchronously, the internal electric field under the mesh will suppress the emission of SE from the insulator surface, and electrons from the insulator do not directly see the chamber wall due to the configuration of the electric field around the mesh. The reduction of the surface potential will be weakened. Furthermore, the model can be used to optimize the height and dimension scale of the assisted mesh for special insulator and initial plasma conditions, and apply optimization to mesh-assisted PIII on insulator for optimum dose uniformity and implanted ion energy. For mesh-assisted PIII, the ability to plasma implant insulating materials broadens the applications tremendously and the primary beneficiaries are the SOI, biomedical and polymeric industries.

4. Conclusion

In summary, a method utilizing PIC model considering SEE as a function of ion instantaneous incident energy has been developed to simulate mesh-assisted PIII on insulator. The dynamic sheath model will yield some insight on the process and is quite powerful combining with experimental verification. On 5 mm thick polymer substrate, the mesh-assisted aluminum PIII coating is achieved with excellent adhesion strength and no shadow effect. Our results indicate that mesh-assisted PIII can improve the equivalent surface potential, suppress the emission of SE and provide better implantation dynamics for ions implantation on insulator.

Acknowledgements

The work was jointly supported by the National Natural Science Foundation of China (No. 50904020), the Science and Technology Innovation Research Project of Harbin for Young Scholar (No. 2009RFQXG050), the Fundamental Research Funds for the Central Universities (No. HIT. NSRIF. 2012007) and the China Postdoctoral Science Foundation (Nos. 20090460883 and 201003419).

References

[1] A. Lacoste, F. Le Coeur, Y. Arnal, J. Pelletier, C. Grattepain, Surf. Coat. Technol. 135 (2001) 268–273.
[2] J. Pelletier, F. Le Coeur, Y. Arnal, A. Lacoste, A. Straboni, Surf. Coat. Technol. 136 (2001) 7–15.
[3] A. Lacoste, J. Pelletier, Nucl. Instrum. Methods Phys. Res. B 208 (2003) 260–266.
[4] P.K. Chu, J. Vac. Sci. Technol. B 22 (2004) 289–296.
[5] T.W.H. Oates, M.M.M. Bilek, J. Appl. Phys. 92 (2002) 2980–2983.
[6] G.A. Emmert, J. Vac. Sci. Technol. B 12 (1994) 880–883.
[7] S.Y. Allan, D.R. McKenzie, M.M.M. Bilek, Plasma Sources Sci. Technol. 19 (2010) 045002.
[8] B.P. Linder, N.W. Cheung, IEEE Trans. Plasma Sci. 24 (1996) 1383–1388.
[9] X.B. Tian, R.K.Y. Fu, P.K. Chu, S.Q. Yang, Surf. Coat. Technol. 196 (2005) 162–166.
[10] X.B. Tian, S.Q. Yang, Y.X. Huang, P.K. Chu, R.K.Y. Fu, J. Phys. D: Appl. Phys. 37 (2004) 50–54.
[11] R.K.Y. Fu, X.B. Tian, P.K. Chu, Rev. Sci. Instrum. 74 (2003) 3697–3700.
[12] R.K.Y. Fu, P.K. Chu, X.B. Tian, J. Appl. Phys. 95 (2004) 3319–3323.
[13] A. Kondyurin, B.K. Gan, M.M.M. Bilek, K. Mizuno, D.R. McKenzie, Nucl. Instrum. Methods Phys. Res. B 251 (2006) 413–418.
[14] R.C. Powles, D.R. McKenzie, N. Fujisawa, D.G. McCulloch, Diamond Relat. Mater. 14 (2005) 1577–1582.
[15] A.R. Marcondes, M. Ueda, K.G. Kostov, A.F. Beloto, N.F. Leite, G.F. Gomes, C.M. Lepienski, Braz. J. Phys. 34 (2004) 1667–1672.
[16] K.G. Kostov, M. Ueda, I.H. Tan, N.F. Leite, A.F. Beloto, G.F. Gomes, Surf. Coat. Technol. 186 (2004) 287–290.
[17] R.C. Powles, D.T.K. Kwok, D.R. McKenzie, M.M.M. Bilek, Phys. Plasmas 12 (2005) 093507.
[18] K. Nakamura, M. Tanaka, H. Sugai, Plasma Sources Sci. Technol. 11 (2002) 161–164.
[19] X.B. Tian, C.Z. Gong, Y.X. Huang, H.F. Jiang, S.Q. Yang, R.K.Y. Fu, P.K. Chu, Appl. Phys. Lett. 93 (2008) 191501.
[20] H. Rothard, R. Moshammer, J. Ullrich, H. Kollmus, R. Mann, S. Hagmann, T.J.M. Zouros, Nucl. Instrum. Methods Phys. Res. B 258 (2007) 91–95.